

# ENHANCING 3D MODELING EFFICIENCY VIA SEMI-AUTOMATIC POINT CLOUD SEGMENTATION AND MULTI-LOD MESH RECONSTRUCTION

*Antonella Musicco\*, Michele Buldo\*, Nicola Rossi\*, Riccardo Tavolare\*, Cesare Verdoscia\**

\*Department of Civil, Environmental, Land, Construction and Chemistry, Polytechnic University of Bari.

## Abstract

The accuracy of 3D models in historical buildings is a debated topic due to the increasing demand for digital documentation and the need for automated post-processing methods to reduce manual labor and improve data analysis. The proposed method aims to improve 3D reconstruction efficiency for complex geometries exemplified by the Ognissanti Church of Trani (XII century), Italy. The methodology includes point cloud segmentation and classification algorithms, (RANSAC and Random Forest) to isolate architectural elements. The segmented portions undergo processing utilizing three 3D reconstruction algorithms: Alpha-Shape, Ball-Pivoting, and Poisson Surface Reconstruction. Customized settings enable polygonal meshes with varying levels of detail. Visual Programming Language operations refine the resulting meshes in terms of triangulation and computational efficiency, ensuring a high level of fidelity and applications in HBIM framework.

## Keywords

Cultural Heritage, Point Cloud, Machine Learning, RANSAC, Mesh Reconstruction, Level of Detail, VPL

## 1. Introduction

The precision of 3D building models has become a contentious research topic within the realm of historical architecture. Over the past few decades, there has been a growing need for digital documentation serving diverse objectives. Advancements in technology have facilitated the development of intricate, reality-based 3D representations that accurately depict the current state of buildings, sculptures, and artifacts. Such models find utility across a range of applications, including building documentation (Clini et al., 2018) (Leserri & Rossi, 2023), virtual reality experiences (Cicerchia & Solima, 2021; De Fino et al., 2020), and cost-effective documentation (Musicco et al., 2023). Terrestrial Laser Scanning (TLS) and digital photogrammetry allow the creation of extensive sets of detailed 3D scenes represented as point clouds. These geometric structures are becoming increasingly essential to support the 3D modeling process (Florio et al. 2019) (Yang, Shishuo, & Wei, 2022).

However, the process has two main drawbacks: it requires a significant time investment and it generates an excessive amount

of data, as 3D scans (regardless of whether they are based on TLS or close-range photogrammetry) contain much more information than is actually necessary for 3D modeling, for these reasons there is the need to consolidate methods to streamline post-processing of point clouds, which will reduce the time and manual activities related to discretization, classification and analysis of data contained in the point clouds (Cotella, 2023). Actually, from a methodological standpoint, the deconstruction of the building heritage, considering its plasticity, and the grammar of geometric forms, serves as the starting point for defining the variable elements of the parametric or solid model.

The semantic classification of architectural elements, prior to the modeling phase, is a fundamental step to avoid creating objects devoid of architectural significance. Furthermore, solid or parametric modeling of Cultural Heritage (CH) objects, often altered by the time that has passed since their original form, can introduce an excessive level of approximation which leads to errors in the documentation of the state of the places (Capone & Lanzara, 2019).

The document outlines a parametric-assisted method for dimensional control of reconstruction of three-dimensional models for the built heritage. Research implements emerging open sourcing and cloud computing paradigms using freely available software technologies (CloudCompare and Python) that can facilitate accessibility to potential asset reuse. The proposed workflow is applied to the Ognissanti Church of Trani (Italy, XII century) which contexts entail a substantial volume of 3D points, diverse geometries, intricate decorations, and irregular architectural elements.

The process of segmentation of the whole dataset and the 3D reconstruction by meshing algorithms of a column of the central nave is described. Different kinds of algorithms have been applied for the segmentation and the classification. The point cloud segmentation activity was semi-automated by integrating the use of two algorithms, Random Sample Consensus (RANSAC) (Fischler & Bolles, 1981; Schnabel et al., 2007) and Random Forest (Letard et al., 2024), to isolate the architectural elements present in the dataset.

For complex elements such as columns, a meticulous study of 3D reconstruction parameters was conducted using meshing algorithms, including Alpha-Shape, Ball-Pivoting, and Poisson Surface Reconstruction, to ensure finer control over dimensional characteristics at multiple levels of detail, tailored to specific requirements (Bernardini et al., 1999). In an HBIM context optimization of polygonal models in terms of triangulation and parametric association with architectural elements was facilitated through the use of Visual Programming Language (VPL) tools such as Dynamo in Autodesk Revit.

## 2. State of Art

The surveying activity of architectural survey through digital methodologies acquires the position of points collected in the so-called clouds which are then represented in three-dimensional models from which traditional two-dimensional drawings are extracted (Di Giuda & Villa, 2016). These products allow for the preservation of a significant amount of information regarding the surveyed objects. Point clouds are sets of thousands of points, each of which is identified by spatial coordinates and colorimetric information.

The amount of data processed during digital surveying requires developing methods for automating semantic analysis processes of point clouds and solid, parametric 3D reconstruction.

In the following sections, a focus is presented on literature regarding point cloud segmentation and classification algorithms (Sec 2.1), as well as mesh processing (Sec 2.2).

### 2.1 Segmentation and classification methods for enhancing modeling process

The segmentation methods of point clouds commonly used in literature to support the modeling process can be divided into two main categories: traditional methods (region growing, model-fitting, clustering, etc.) and innovative methods which introduce artificial intelligence algorithms (machine learning, deep learning, etc.) (Zhao et al., 2023). Among the traditional approaches, we can distinguish two categories more commonly used in the field of CH: region growing and model fitting.

The working principle of region growing is based on the growth of regions from initial points called seeds. The algorithm iteratively evaluates adjacent points to the seeds and grows the region based on similarity. It has been widely used in literature for image segmentation and for segmenting planar structures in point clouds (Sakamoto et al., 2020). Pérez-Sinticala et al. (2019) enhanced a hybrid method based on region growing algorithm and primitive fitting by Sample Consensus for segmenting the front wall and rooftop. However, it is the least suitable for segmenting complex and articulated point clouds. Three main limitations are recognized due to (Kang et al., 2020): (1) the erroneous selection of initial seed points, (2) the presence of numerous parameter settings, and (3) the frequent occurrence of over-segmentation or under-segmentation issues.

Model-fitting algorithms assist in identifying correspondences within the point cloud concerning geometric primitives (planes, spheres, cylinders, etc.). Among these, the most prevalent is the Hough Transform (HT) (Duda & Hart, 1972), and Random Sample Consensus (RANSAC) (Fischler & Bolles, 1981). HT was initially applied to point clouds for facilitating the identification of roof faces. Subsequently, its methodology was broadened to encompass the extraction of additional 3D geometric structures such as cylinders and spheres (Rabbani & Heuvel, 2005). The RANSAC algorithm was originally introduced by Fischler and Bolles for image detection purposes. Schnabel et al. (2007) later extended its

application to the detection of fundamental shapes, including cones, spheres, cylinders, and planes, within 3D point clouds.

Notable extensions of RANSAC are Maximum Likelihood Estimation SAmple and Consensus, M-estimator SAmple and Consensus, and Progressive Sample and Consensus (Grilli et al., 2017).

In recent investigation applied to CH, the effectiveness of RANSAC on point cloud has been tested for the extraction of geometric primitives of architectural components, such as those of a Dorik Greek temple (Kyruakaki-Grammatikaki et al., 2022), or different types of masonry vaults (Buldo et al., 2023).

However, region growing and model fitting algorithms facilitate the subdivision of point clouds into homogeneous regions in less complex datasets. In the CH domain, however, the complexity and irregularity of shapes necessitate more flexible methods. Furthermore, the classification of segmented points remains a manual task and is entrusted to the operator.

Machine Learning (ML) and Deep Learning techniques have greatly streamlined the interpretation of digital data, semantic structure, and object identification (Yang et al., 2023). At the core of ML lies the concept that systems can acquire knowledge from data, autonomously recognize patterns, and make decisions with limited human intervention. In the analysis of point clouds using ML, the interpretation of each individual observation (element) relies solely on its correlation with others. Therefore, the basic problem of ML consists in finding the clustering method, namely to find homogeneous groups in a given dataset. Each group is called "cluster" and can be defined as a region in which there are some similarities and differences from the others. The ML approach involves data preprocessing, feature extraction, model training, evaluation, and classification using the trained model. Artificial features of point clouds fall into three categories: statistical features (density, elevation difference, elevation, etc), histogram-based features (mean, standard deviation, etc), and geometric features (linearity, planarity, sphericity, etc.) Commonly used classifiers include Support Vector Machine, Random Forest, and Parsimonious Bayes. Although there are diverse classifiers to choose from, the selection typically hinges on the particular problem at hand and its computational requirements. Random Forest classifiers, favored for their equilibrium between precision and

computational efficiency, are frequently utilized in tasks involving the classification of point clouds. Indeed, in several works examined in the literature applied to historical buildings and temples distributed across European territories, the Random Forest classifier combined with the study of geometric features is the most experimented and utilized. This is because it enables obtaining appreciable results in the identification activities of predetermined categories of architectural elements (such as columns, bases, entablatures, vaults, etc.) through a training set, (Grilli et al., 2019a; Pepe et al., 2022), sometimes also through statistical features (Grilli & Remondino, 2019).

## 2.2 Modelling phase

The creation of three-dimensional surfaces or meshes from point clouds is a widely studied topic in the CH domain. Obtaining a three-dimensional model of an object from images or laser data opens up many possibilities in various sectors, not only in engineering and architecture (Alqudah, 2014). For this reason, researchers have tested various methodologies for surface reconstruction. Some of the most commonly used methods, as analyzed in the research of Khatamian (2016) and Sharma (2023), include the Alpha Shape algorithm (Edelsbrunner & Mucke, 1994), Ball-Pivoting (Bernardini et al., 1999), and Poisson Surface Reconstruction algorithm (Kazhdan et al., 2006). The Alpha Shape algorithm uses a disk to intercept the points of a cloud and create polygons consisting of triangular faces. The Ball-Pivoting algorithm is based on the use of a virtual sphere (ball) with a user-defined radius, which is moved over the point cloud determining the vertices of the triangles that will constitute the mesh (Digne, 2014). The Poisson Surface Reconstruction algorithm, on the other hand, identifies the faces of an object's surface using a vector field (Bolitho et al., 2009). In the realm of CH and its valorization, the use of 3D models composed of surfaces has become increasingly significant, especially for the documentation and representation of more complex architectural elements (Bolognesi & Manfredi, 2024) Furthermore, depending on the type of representation desired, meshes of varying quality can be produced and utilized to optimize file management and processing times (Liang et al., 2023). This can be achieved through the utilization of previously introduced Surface Reconstruction (SR) algorithms, which provide a high level of control over mesh creation properties.

Additionally, these more detailed models can enrich simple 3D modeling or even information models such as those associated with BIM methodology (Yang et al., 2019; Vosselman et al., 2001).

### 3. Methodology

#### 3.1 3D Data segmentation and classification

One objective of this work is to semantically segment 3D data obtained during the survey,

isolating morphological units to streamline 3D modeling tasks. This is achieved by leveraging the semantic description of its components through classification based on types of constructive elements from the ontological taxonomy of the Art & Architecture Thesaurus of the Getty Research Institute. This approach is chosen due to its alignment with the principles of classical architecture and its applicability across a broad temporal range. In the original point cloud, the categories of elements shown in Fig. 1 were distinguished.

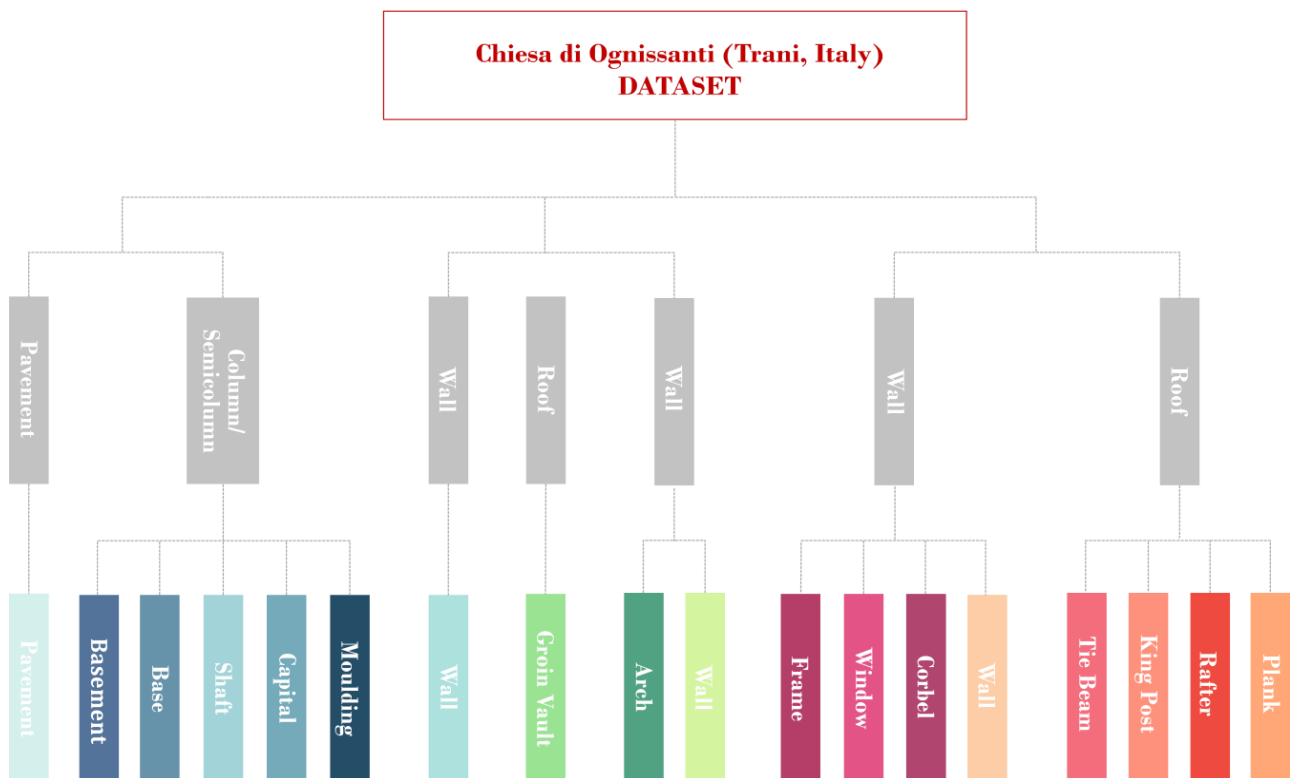


Fig. 1 Taxonomy of architectural elements in the adopted dataset

The point cloud was segmented by combining the use of model-based algorithms (such as RANSAC) for regular and planar architectural elements, and Machine Learning (Random Forest) for serial and more complex ones. The wall facings, the floor, and the vaults of the side naves were segmented using RANSAC.

The process involves a recursive comparison of geometric primitives (plane, cone, cylinder, sphere, torus) with real ones, which stops with the extraction of the set of points that best approximates the preselected shape. In this context, RANSAC was executed using the CloudCompare software (Girardeau-Montau, 2020), choosing planes and cylinders as reference

primitives. A minimum sampling radius for the cylinder was chosen based on the geometry of the smallest element to be extracted. In this context, the half-light of the vault. (1,2-1,5m). For the portion of the point cloud related to the central nave, a Machine Learning method, Random Forest in CloudCompare via the 3DMASC plugin (Letard et al., 2024), was chosen because machine learning improves the segmentation process by automating classification based on learned models, especially in the case of datasets containing serial elements, as in this context where columns, trusses, and decorative features are recurring elements. The use of Random Forest in 3DMASC allows for the management of

multidimensional data and sets of different features (RGB, intensity, number of returns, planarity, linearity, sphericity, etc.).

Segmentation was initiated using the multi-level feature detection method proposed by (Dimitrov & Golparvar-Fard, 2015) following five main phases: (a) selection of point neighborhoods based on a reference radius, (b) extraction of geometric features on the entire dataset, (c) selection of the most performing features for architectural component detection, (d) manual annotation, and finally, (e) classification (Grilli et al., 2019b).

One crucial aspect concerns delineating

neighborhoods for individual points within a 3D point cloud. Different approaches, such as utilizing spherical or cylindrical neighborhoods, either separately or in combination, have been utilized. The selection of neighborhood type and the calibration of the scale parameter, whether based on prior knowledge or a data-driven methodology, can profoundly influence the outcomes of classification tasks.

For this purpose, the selection of the spherical neighborhood radius was carefully calibrated in relation to the sizes of the objects to be identified. For example, the average radius of the tori composing the base of the columns is approximately 0.04 meters.

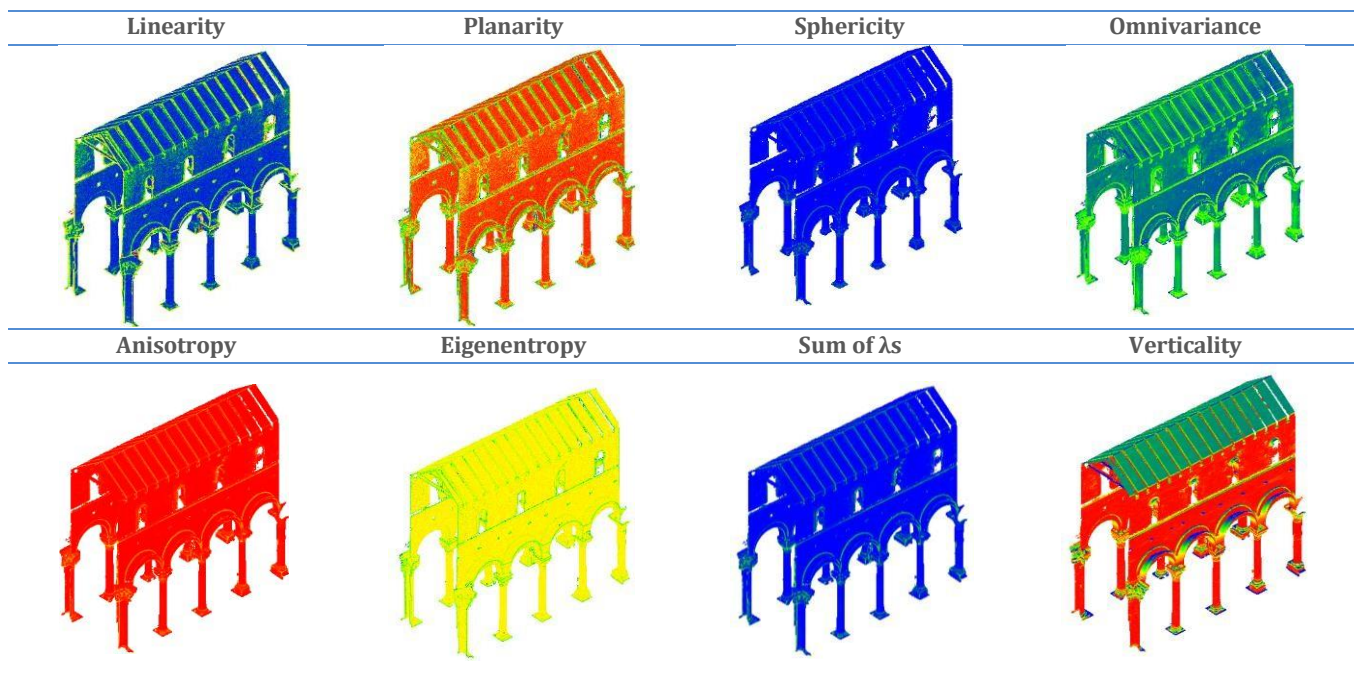


**Fig. 2** Geometric features extracted in CloudCompare

Once neighborhoods are established, the extraction of features (radiometric, geometric, or spectral) becomes the next step (Dimitrov & Golparvar-Fard, 2015; Weinmann et al., 2017). These features capture the spatial arrangements of neighboring points and provide critical information for classification. In this paper, geometric features have been used, based on eigenvalues  $\lambda_1, \lambda_2, \lambda_3$ , as 3D shape descriptors extracted from the covariance matrix as described in (Blomley et al., 2014):

- $Linearity = \frac{\lambda_1 - \lambda_2}{\lambda_1}$
- $Planarity = \frac{\lambda_2 - \lambda_3}{\lambda_1}$
- $Sphericity = \frac{\lambda_3}{\lambda_1}$

- $Omnivariance = \sqrt[3]{\lambda_1 \lambda_2 \lambda_3}$
- $Anisotropy = \frac{\lambda_1 - \lambda_3}{\lambda_1}$
- $Eigenentropy = -\sum_{i=1}^3 \lambda_i \ln(\lambda_i)$
- $Sum\ of\ Eigenvalues = \sum_{i=1}^3 \lambda_i$

In addition to geometric features, parameters such as verticality and point height in the point cloud (Z coordinate) were also considered.

The choice of features is crucial, as it directly affects the classifier's ability to differentiate between classes. Furthermore, it's crucial not to disregard the significance of individual features, as not all hold equal importance for classification purposes. A range of methods, such as filter-based techniques, are employed to assess feature

relevance, aiding in the identification of the most critical features for the given task. These techniques analyze correlations, statistical variances, information gain, and other criteria to prioritize features based on their relevance.

From the analysis of geometric characteristics performed in CloudCompare (Fig. 2), the following emerges:

a) Verticality and Linearity are the features that best distinguish the constructive elements, highlighting the vertical trend of shafts, capitals, and the horizontal trend of vaults and arches;

b) The curvature of the arches was better described by Surface Variation, Sphericity, and Omnivariance;

c) Sum of Eigenvalues, Eigentropy, and Anisotropy yielded less significant results.

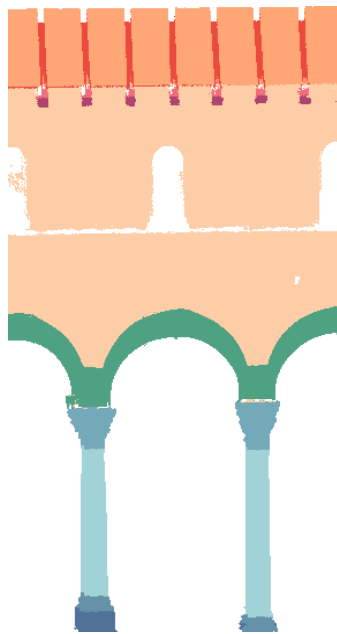


**Fig. 3** Training set of the central nave

Random Forest, in 3DMASC, has been applied on the remain portion of the dataset of the central naves composed of 38,643,593 points. A part of this portion was taken as the training set (Fig. 3), consisting of 10.453.976 points where ten semantic classes of elements were distinguished (wall, corbel, rafter, tie beam, molding, arch, capital, shaft, base, basement). The remaining part of the dataset from the central nave was used to test and validate the training results using the precision metrics described in section 3.1.1.

### 3.1.1 Validation Test

Correct and incorrect predictions are tallied and categorized by class within a confusion matrix

which is a specialized table format for visualizing algorithm performance. Each row denotes instances in the actual class (ground truth), and each column represents instances in a predicted class. Confusion matrix is not a direct performance measure; the accuracy metrics rely on the data within the confusion matrix, that are:

Precision is the ratio of positive observations correctly predicted to the total positive observations predicted.

$$Precision = \frac{TP}{(TP+FP)} \quad (1)$$

Accuracy refers to the ratio of correctly classified data to the total number of points.

$$Accuracy = \frac{TP+TN}{(TP+TN+FP+FN)} \quad (2)$$

Recall is the ratio of positive observations to all observations in the actual class.

$$Recall = \frac{TP}{(TP+FN)} \quad (3)$$

F1 Score is the weighted average of Precision and Recall.

$$F1\ Score = \frac{2*(Recall*Precision)}{(Recall+Precision)} \quad (4)$$

$TP$  = true positive,  $TN$  = true negative,  
 $FP$  = false positive,  $FN$  = false negative.

### 3.2 Mesh optimization

One of the main challenges in computer graphics related to digital documentation of Cultural Heritage is the efficient management of 3D data to represent complex objects in an optimized and computationally manageable manner. In this context, an experiment was conducted on 3D reconstruction defined by polygonal meshes, employing an approach developed using three well-known algorithms – Alpha Shape, Ball-Pivoting, and Poisson Surface Reconstruction – within a Python environment.

Starting from individual regions of previously segmented and classified point clouds, the aim was to enable the creation of representations that can be reusable for subsequent developments, such as Historic Building Information Modeling (HBIM), by defining meshes for each implemented algorithm with varying levels of detail (LOD), from the lowest to the highest level.

As a case study, a column representing the main nave of the church was considered, semantically divided into various portions such as basement, base, shaft, and capital.

Regarding the first mentioned algorithm, the

Alpha Shape, a set of three-dimensional points is represented by a polygonal structure called 'alpha shape', constructed using disks with radii inversely proportional to a parameter alpha ( $\alpha$ ) which controls the algorithm's sensitivity to point distribution (Crisan et al., 2024). This structure approximates the global shape of the point set by including points lying within these disks while excluding those outside. The variation of alpha modifies the radius, the complexity of the generated shape, and hence the detail of the resulting mesh: smaller  $\alpha$  values result in disks with larger radii and include a greater number of points, while larger  $\alpha$  values determine a greater approximation of the shape and a decrease in detail. Therefore, an approach based on LOD subdivision was defined based on the search for different alpha values.

Starting from the set of segmented and subsampled point clouds at 3 mm, the research focused on determining  $\alpha$  parameter while considering the local densities of points within the three-dimensional dataset. The density of a point, in this regard, was considered as the number of surrounding points within a certain predefined radius; therefore, calculating local densities is an operation critical for understanding the spatial distribution of points in the cloud. This definition implies that densely clustered points will have higher density values compared to isolated or scattered points.

To calculate local densities, the K-d Tree algorithm was employed, which enables efficient

search for the nearest neighbors of each point in the cloud. In practice, for each point, a set of surrounding points within a predefined radius is determined. To establish the search radius, the decision was made to utilize the average distance between the nearest points in the cloud, in order to provide a reasonable measure of the spatial scale of the data. Once the search radius is determined, the local search for neighbors is performed, and the number of points found within this radius represents the local density of the point.

The three alpha values used, which were computed proportionally to the local densities, are respectively  $\alpha_{LOD1}$  considered as the inverse of the minimum density,  $\alpha_{LOD2}$  the inverse of the average density and  $\alpha_{LOD3}$  the inverse of the maximum density. These alpha values are then used in the Alpha Shape algorithm to generate three meshes with different detail sensitivities, adapted to the distribution of points in the three-dimensional cloud.

Additionally, an extra LOD ( $\alpha_{LOD4}$ ) was considered by defining the parameter  $\alpha$  as the maximum distance between points, essentially considering the smallest possible radius to define the shape of the disks in the algorithm. This decision was made to maximize sensitivity to details in surface reconstruction. The definition of the adopted parameters, along with their respective values, is summarized in Table 1.

**Tab. 1:** Alpha parameter for different LODs using Alpha-Shape algorithm

Alpha	Equation	Value	
$\alpha_{LOD1}$	$\alpha_{LOD1} = \frac{1}{\rho_2} = \frac{1}{\text{minimum density}}$	Basement	1.000
		Base	1.000
		Shaft	1.000
		Capital	1.000
$\alpha_{LOD2}$	$\alpha_{LOD2} = \frac{1}{\rho_2} = \frac{1}{\text{mean density}}$	Basement	0.533
		Base	0.539
		Shaft	0.550
		Capital	0.530
$\alpha_{LOD3}$	$\alpha_{LOD3} = \frac{1}{\rho_3} = \frac{1}{\text{maximum density}}$	Basement	0.167
		Base	0.143
		Shaft	0.143
		Capital	0.143
$\alpha_{LOD4}$	$\alpha_{LOD4} = \text{maximum distance}$	Basement	0.023
		Base	0.020
		Shaft	0.012
		Capital	0.013

Regarding the utilization of the Ball Pivoting algorithm, a random point within the dataset is chosen as a starting point for generating a three-dimensional mesh. The algorithm employs rotating spheres around points in a dataset to initialize triangles based on three points. When a sphere touches other points in the set, new triangles are created. This process continues until all points have been explored, generating a continuous surface in the form of a triangular mesh.

The parameter of the sphere radius used during this process controls the sensitivity to details and the computational complexity of the algorithm: a smaller radius produces a more detailed mesh but is computationally more demanding, while a larger radius reduces complexity at the expense of detail precision (Saffi

et al., 2024).

For this experimentation, a radius was defined for each of the three defined LODs, corresponding respectively to the minimum, maximum, and average distance between the nearest neighbors in the point cloud. Additionally, a fourth LOD was added, equal to the average density between points multiplied by an empirical coefficient commonly used in the literature. Indeed, since in some regions of the point cloud, the density may vary significantly, multiplying the average density by a coefficient can help mitigate the effect of scattered or irregularly distributed points in the point cloud and can improve the algorithm's ability to accurately reconstruct surfaces even in regions with variable point densities.

Below are the different radius values adopted for 3D reconstruction using the Ball- Pivoting algorithm (Table 2).

**Tab.2:** Radius parameter for different LODs using Ball-Pivoting algorithm

Radius	Equation	Value	
$\rho_{LOD1}$	$\rho_{LOD1} = \textit{minimum distance}$	Basement	0.003
		Base	0.003
		Shaft	0.003
		Capital	0.003
$\rho_{LOD2}$	$\rho_{LOD2} = \textit{mean distance}$	Basement	0.003
		Base	0.003
		Shaft	0.003
		Capital	0.004
$\rho_{LOD3}$	$\rho_{LOD3} = \textit{maximum distance}$	Basement	0.023
		Base	0.020
		Shaft	0.012
		Capital	0.013
$\rho_{LOD4}$	$\rho_{LOD4} = 3 * \textit{mean distance}$	Basement	0.010
		Base	0.010
		Shaft	0.010
		Capital	0.011

The third algorithm utilized is Poisson Surface Reconstruction, which serves as a method for reconstructing smooth and continuous surfaces from irregular 3D scanning data, employing an implicit meshing approach. This algorithm leverages a vector field derived from the distribution of points in the point cloud, reflecting local variations in point density and correlated with the surface gradient. The use of a data structure such as the octree optimizes the computation of this vector field, influencing the resolution and accuracy of the reconstruction.

The Poisson equation is solved to determine the shape of the initial object, enabling the

generation of a precise mesh that conforms to the original points. A key parameter is the 'depth' of the octree, indicating the maximum number of levels of tree subdivision for partitioning the three-dimensional space (Kazhdan et al., 2007; Bassier et al., 2020).

A higher depth value corresponds to a higher level of detail in the mesh. The 'scale' parameter, on the other hand, represents the ratio between the maximum distance between two opposite points within the sample bounding cube and the diameter of this cube. Smaller scale values allow for greater precision in surface details but may increase computation time and memory

requirements, while larger values have the opposite effect.

In this study, an empirical value of the scale parameter, set to 1.1, was chosen for each segmented point cloud and for each LOD. Greater emphasis was placed on defining the depth parameter, which was calculated semi-automatically. To this end, a function was initially defined to utilize differences between the coordinates of adjacent points to calculate the Euclidean distances between them, returning the average of these distances, representing the average distance between points in the cloud. Using the average distance as a measure of data density, three depth values influencing the detail of surface reconstruction were subsequently

determined. To achieve this, three scale factors were defined, namely 0.2, 0.1, 0.05, and 0.03, for calculating the depths, computed as the average distance multiplied by the respective scale value.

The calculated depth values were constrained to specific intervals to ensure that each subsequent level captured more details than the previous one, allowing representation of shape variations at different spatial scales (Poux et al., 2020).

For *LOD 1*, a depth range of 3-6 was selected, for *LOD 2* a range of 6-9, for *LOD 3* a range of 9-12, and for *LOD 4* a range greater than 12. In Table 3, the parameters used with the Poisson algorithm are summarized.

**Tab. 3** Depth and Scale parameters for different LODs using Poisson Surface Reconstruction algorithm

ELEMENT	LOD	Scale	Depth
Basement	LOD 1	1.1	3
	LOD 2	1.1	6
	LOD 3	1.1	9
	LOD 4	1.1	12
Base	LOD 1	1.1	3
	LOD 2	1.1	6
	LOD 3	1.1	9
	LOD 4	1.1	12
Shaft	LOD 1	1.1	3
	LOD 2	1.1	6
	LOD 3	1.1	12
	LOD 4	1.1	15
Capital	LOD 1	1.1	3
	LOD 2	1.1	6
	LOD 3	1.1	9
	LOD 4	1.1	13

#### 4. Test on building elements

##### 4.1 Initial Dataset

The workflow was applied to the Romanesque Church of Ognissanti in Trani (Italy), dating back to the 12th century (Fig. 4).

The building, of reduced dimensions, is characterized by a porticoed entrance and a rectangular hall divided into three naves ending with three semicircular apses. The naves are separated by twelve composite granite columns on which the double lancet arches are supported. The central nave is covered by a system of wooden trusses while the side naves are topped by pointed arch vaults.

The survey was conducted using the Faro Focus 3D 120 CAM2 Laser Scanner which has a range of up to 120 meters, and defines a

systematic measurement error (ranging error) between 10- 25 m of  $\pm 2$  mm, and a resolution camera of 70- megapixel. A total of 55 scans were performed (19 on the external perimeter and 36 inside), aligned and post-processed in Recap Pro® to obtain an overall point cloud of 307,148,542 points.

The workflow developed in this contribution was applied to a portion of the point cloud. External environments and the entrance portico were excluded, focusing solely on the indoor environment. Previously, furnishing elements (benches, light fixtures, statues, etc.) were removed.

Additionally, in CloudCompare, duplicate points were eliminated, and noise was removed through the SOR filter, Resulting in a final dataset of 77.658.165 points.



**Fig. 4** Internal view of Ognissanti Church (XII century), Trani, Italy

#### 4.2 Dataset segmentation and classification

The initial dataset segmentation saw the use of two algorithms RANSAC and Random Forest. RANSAC has made it possible to locate and isolate the simplest architectural elements such as walls, vaults, and floors (Fig. 5). The result of the segmentation has allowed to optimize in terms of time, moreover, the next operation, that is the extraction of the dataset to submit to Random Forest.

The results of Random Forest segmentation were evaluated using the precision metrics (1), (2), (3), (4) described in paragraph 3.1.1 visible in the Table 4. For Random Forest to be effective and generalize to new data, the quality of the training set is crucial.

The diversity, representativeness, and size should be sufficient to capture variations without overfitting. Appreciable results have been achieved due to the seriality and repetition of the constructive elements in the examined dataset, with a total average of 74,31% (1), 66,39% (2), 85,41% (3), and 74,27% (4).

In the context of point cloud applications, the Random Forest algorithm effectively manages the scale of segmentation details and semantic classification allowing flexibility in the selection of geometric characteristics.



**Fig. 5** Wall, floor, and vaults segmented via RANSAC

The classes whose segmentation has had better results are those represented by elements repeated in the dataset in a more or less homogeneous way such as "Wall", "Arch", "Shaft", and "Base".

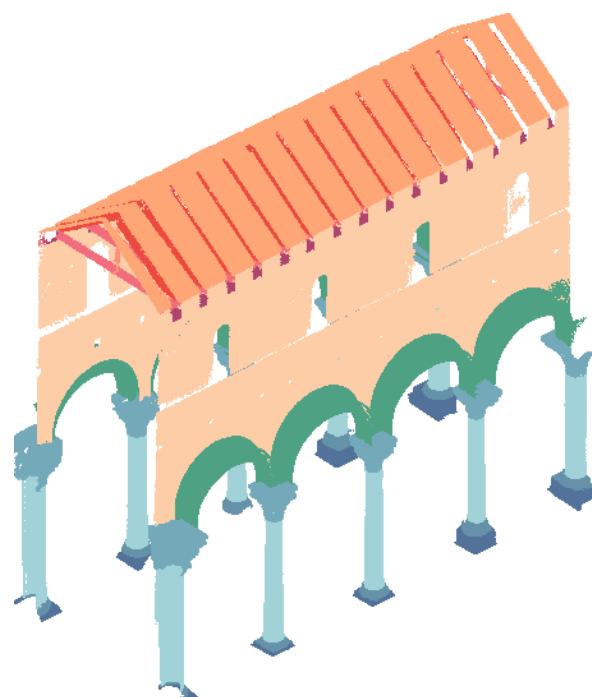


**Fig. 6** Central nave segmented through Random Forest

Even the classes concerning helmets in trusses (corbel, rafter, tie beam) have been correctly classified, however the result of the segmentation was conditioned by an initial cloud full of noise due to the distance of the elements from the laser scanner in the process of acquisition and the

proximity to glass materials present on the neighboring windows. The capitals and basement were segmented elements less precisely than the

rest due to their heterogeneity in the initial dataset (Fig. 6).

**Tab. 4:** Random Forest application performance

	Wall	Corbel	Rafter	Tie beam	Molding	Arch	Capital	Shaft	Base	Basement
Accuracy	92,41%	62,14%	65,33%	51,70%	67,20%	81,68%	48,90%	88,41%	86,67%	58,70%
Precision	99,90%	49,20%	44,58%	43,68%	49,20%	85,38%	32,19%	87,70%	72,13%	59,90%
Recall	98,35%	61,63%	80,45%	80,50%	73,63%	92,17%	54,94%	94,08%	80,00%	58,38%
F1	95,52%	65,20%	63,37%	57,37%	65,20%	89,1%	48,08%	90,78%	83,81%	41,13%

### 4.3 Mesh optimization results

To ensure accurate control over the geometric conformity of the meshes in relation to the starting point cloud, a Cloud-to-Mesh (C2M) comparison was performed using CloudCompare software. This process facilitated the

identification of any measured discrepancies in meters, accompanied by a statistical evaluation through the calculation of the standard deviation using a Gaussian distribution model (Table 5). A lower standard deviation value indicates greater conformity of the mesh to the point cloud and therefore better definition of details.

**Tab. 5** Standard Deviation values between point cloud and mesh

ELEMENT	LOD	Standard Deviation		
		Alpha Shape	Ball-Pivoting	Poisson
Basement	LOD 1	0.006122	0.000944	0.010584
	LOD 2	0.005657	0.001061	0.002235
	LOD 3	0.003758	0.000596	0.001573
	LOD 4	0.001852	0.002380	0.001571
Base	LOD 1	0.021119	0.000964	0.014638
	LOD 2	0.019206	0.001114	0.002449
	LOD 3	0.005815	0.000478	0.001782
	LOD 4	0.001632	0.002501	0.001778
Shaft	LOD 1	0.002628	0.000413	0.034736
	LOD 2	0.002267	0.000425	0.001752
	LOD 3	0.001422	0.001272	0.000860
	LOD 4	0.000350	0.001187	0.000860
Capital	LOD 1	0.025169	0.001169	0.025429
	LOD 2	0.022882	0.001157	0.003028

In general, the standard deviations are relatively high for lower LODs and tend to decrease as LOD increases for most architectural elements when using the Alpha Shape algorithm (). This suggests that the Alpha Shape algorithm may initially produce meshes with lower definition but improves as the level of detail is increased.

Regarding the results obtained with the Ball-Pivoting algorithm, an opposite trend to the first approach is observed (Fig. 8). The standard deviations are relatively low for lower LODs and tend to increase as LOD increases for most architectural elements. The variation in standard deviations is influenced by the mesh conformity to the point cloud and the presence of holes or gaps,

especially in the first two LODs. As LOD increases, the algorithm might overly fit the mesh to the input data, causing overfitting and generating non-significant details, albeit with a continuous surface.

The Poisson Surface Reconstruction algorithm demonstrates better consistency in results with standard deviations often lower than those of other algorithms, especially for higher LODs. This suggests that the Poisson algorithm produces meshes with more accurate definition, particularly when using higher depth levels (Fig. 9).

The deduced results can also be evaluated qualitatively, focusing on the most representative and geometrically complex element of the column, namely the capital.

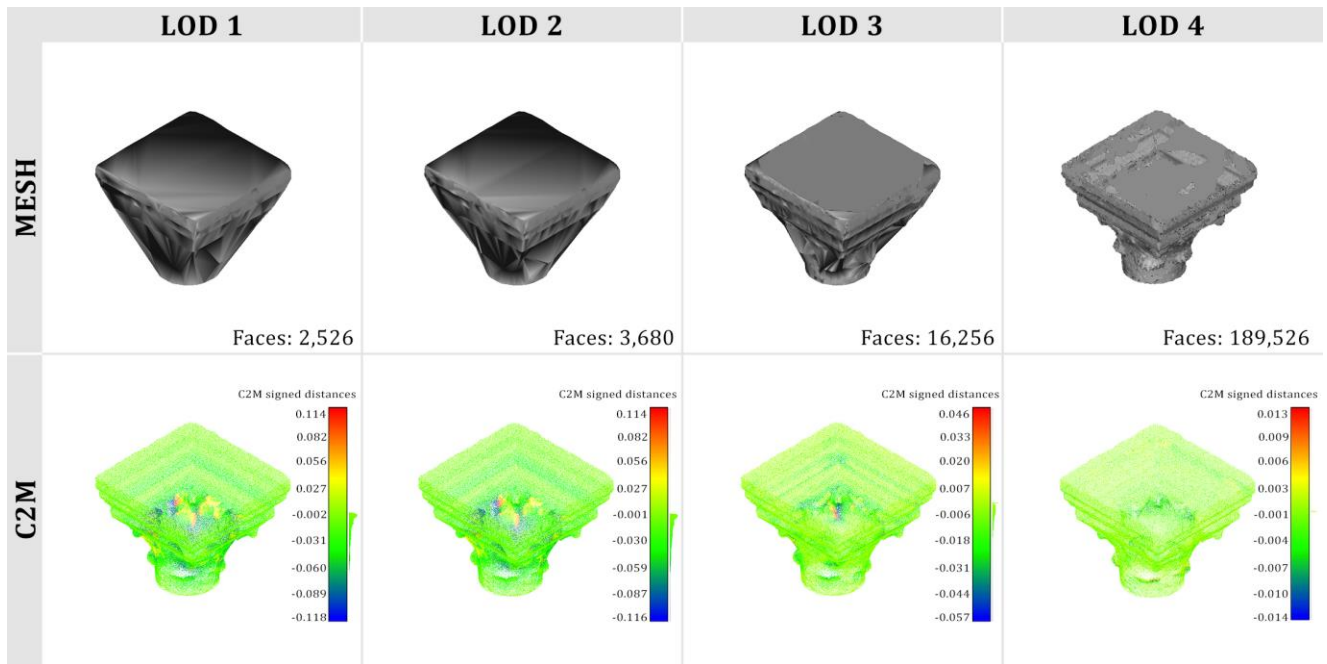


Fig. 7 Multi-LOD mesh visualization with the Alpha Shape algorithm (top) and Cloud-to-Mesh distance (bottom)

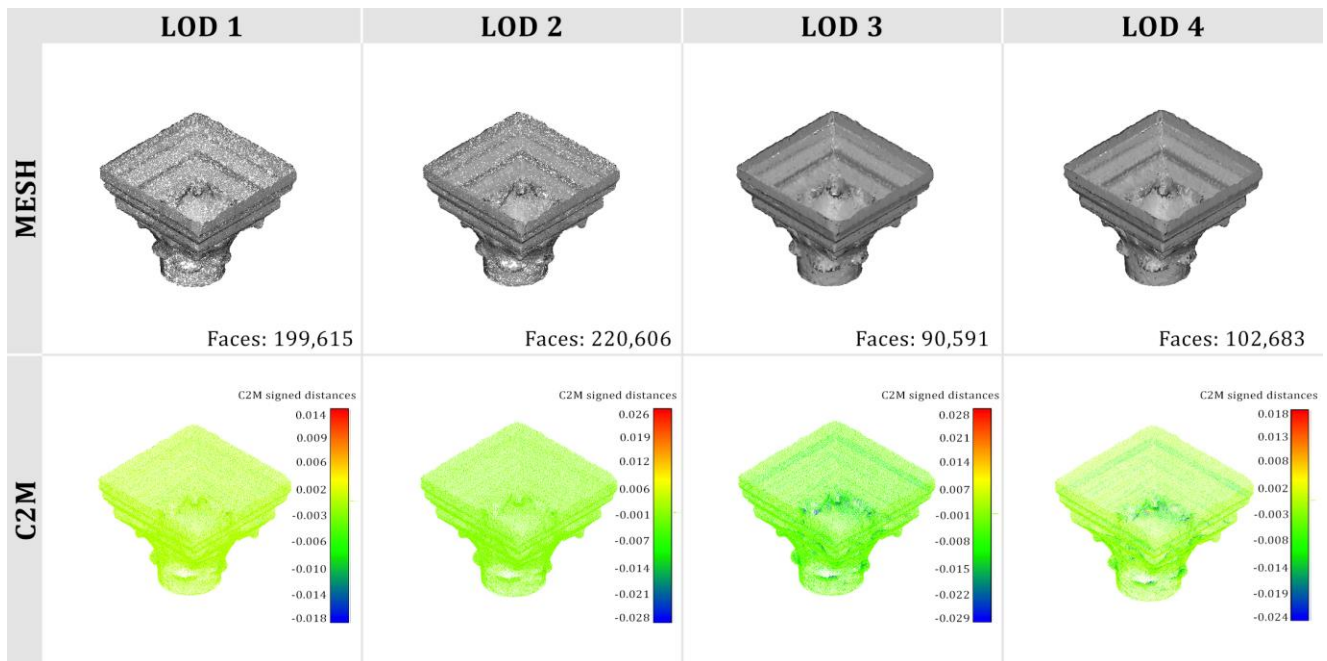
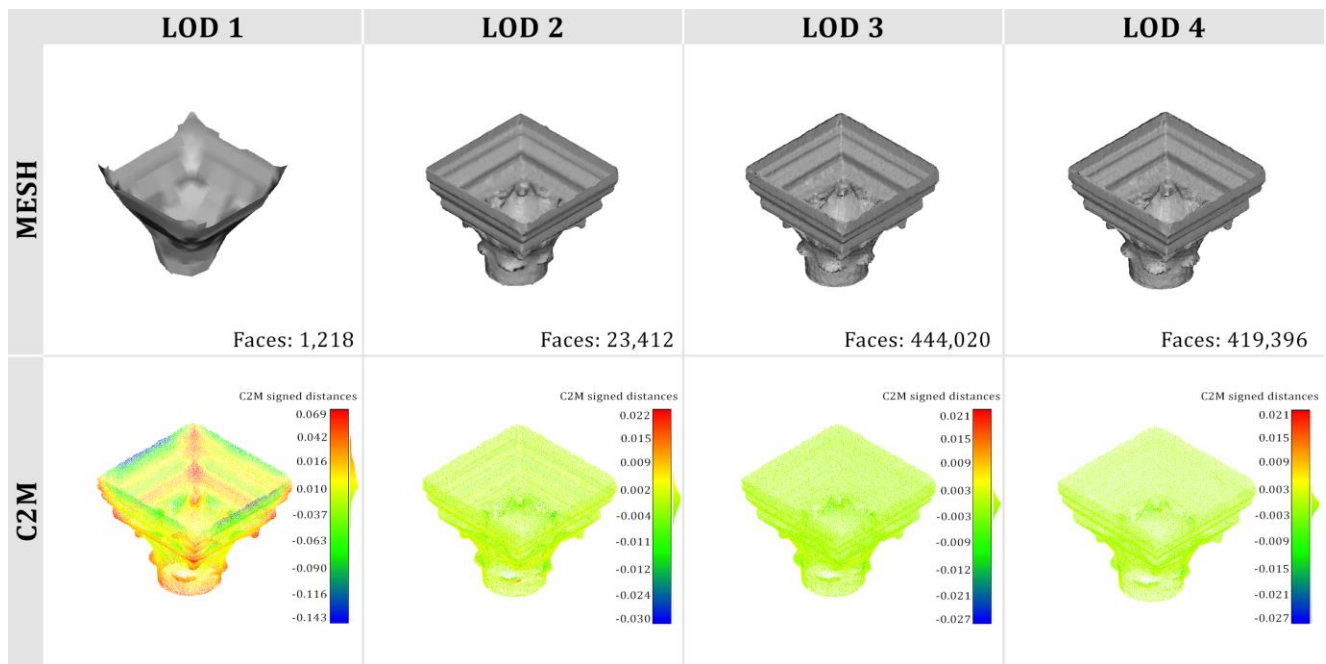


Fig. 8 Multi-LOD mesh visualization with the Ball-Pivoting algorithm (top) and Cloud-to-Mesh distance (bottom)



**Fig. 9** Multi-LOD mesh visualization with the Poisson Surface Reconstruction algorithm (top) and Cloud-to-Mesh distance (bottom)

Examining the meshes obtained with different levels of detail (LOD) for each algorithm used, it's evident that increasing the LOD improves the definition of the mesh. Particularly, when comparing the highly approximated geometries of Alpha Shape and the presence of gaps in the Ball-Pivoting algorithm, the approach adopted with the Poisson Surface Reconstruction algorithm appears to be the most robust in this context.

It is noteworthy that augmenting the level of detail (LOD) leads to a concomitant escalation in the number of facets utilized for mesh reconstruction, owing to the imperative of deploying a greater number of triangles to faithfully depict the object's surface characteristics. Consequently, this engenders an amplification in the volumetric representation of the mesh file, necessitating a commensurate increase in storage capacity to accommodate the augmented geometric intricacies. Nonetheless, an intriguing finding pertains to the discernible reduction in triangulation complexity observed within detail levels 3 (LOD3) and 4 (LOD4), as facilitated by the Ball-Pivoting algorithm, wherein the imposition of radius values equivalent to the maximal and threefold average distances proves instrumental. This strategic adjustment affords a dual benefit of optimizing mesh reconstruction processes while concurrently alleviating computational overhead, thereby manifesting qualitative enhancements. Furthermore,

notwithstanding the computational superiority of LOD 4 achieved through the Poisson algorithm vis-à-vis LOD3, its incremental computational efficacy remains less pronounced compared to antecedent LOD iterations. To address this issue and optimize the computational aspect and geometry of the mesh, especially in HBIM (Heritage Building Information Modeling) contexts (Lanzara et al., 2022) a semi-automated process has been developed for managing the mesh with the highest LOD derived from Poisson Surface Reconstruction, using a VPL script in Dynamo® ( Fig. 10).

The process begins with importing the mesh using the *Mesh.ImportFile* function and offers the option to customize the desired level of detail, in this case opting for the highest level. Subsequently, operations are performed to control the number of polygons in the mesh using *Mesh.Reduce* and to optimize the distribution of triangles through *Mesh.Remesh*. Additionally, the representation scale of the mesh can be adjusted using *Mesh.Scale*.

After completing the mesh processing operations, it is converted into a BIM object using *DirectShape.by Mesh*. This step allows integrating the mesh into a BIM model, where a range of available parameters related to the specific family of the object can be assigned. These parameters may include technical information, such as the material used for construction, structural

properties, performance, or historical information. This level of customization enables adapting the BIM object to the specific project

requirements, ensuring an accurate and comprehensive representation of data within the BIM model context.

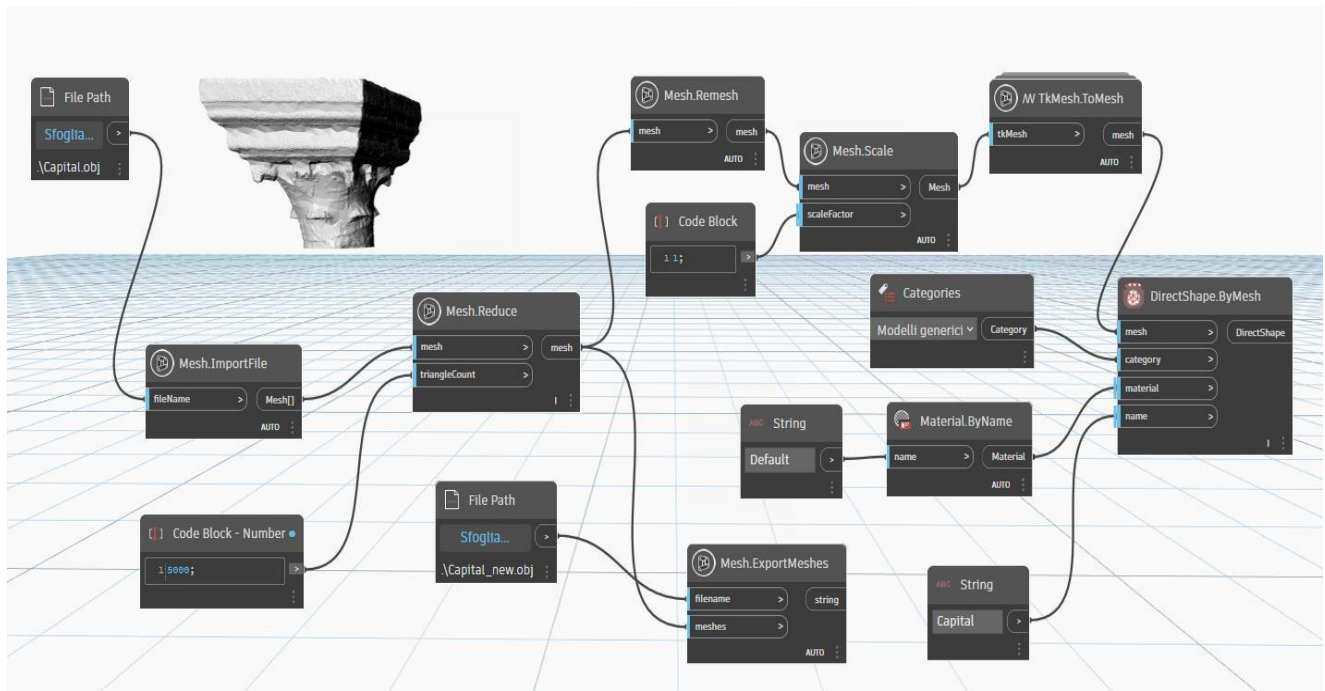


Fig. 10 Mesh optimization via VPL script in Dynamo®

#### 4. Conclusions and future works

In this document, a methodology for managing complex datasets in the field of historical building has been illustrated. Starting from the laser scanner survey, a semi-automatic segmentation and classification was carried out thanks to the use of model-based algorithms (RANSAC) and Machine Learning (Random Forest). Then a comparison was made between three meshing algorithms Alpha Shape, Ball- Pivoting and Poisson Surface Reconstruction to evaluate what best allows to relate the level of detail with the dimensional data required by the needs of representation. RANSAC algorithm allowed to isolate the simplest architectural elements (walls, floors and vaults). For more complex elements (columns, trusses, arches, etc.) it was necessary to use the Random Forest algorithm. The segmented and classified columns were meshed. From the

analysis of the reconstruction of the meshes of segmented points related to a representative column of the church, it is deduced that the Poisson Surface Reconstruction approach offers better consistency in results, especially with higher LOD, while Alpha Shape and Ball-Pivoting show variations in mesh quality depending on the LOD. Increasing the LOD improves the mesh definition but also increases the file size. Therefore, a semi- automated process was created to manage the mesh with maximum LOD, optimizing the computational aspect and the geometry of the mesh in HBIM. The methodology has shown the possibility of saving time modeling complex objects, since the modeling phase is replaced by a semi-automatic process to return objects. The implemented solution can be easily expanded and replicated to manage different architectural elements.

## REFERENCES

- Alqudah, A. (2014). Survey of Surface Reconstruction Algorithms. *Journal of Signal and Information Processing*, 05(03), 63–79. <https://doi.org/10.4236/jsip.2014.53009>
- Bassier, M., Vergauwen, M., & Poux, F. (2020). Point cloud vs. mesh features for building interior classification. *Remote Sensing*, 12(14), 1–26. <https://doi.org/10.3390/rs12142224>
- Bernardini, F., Mittleman, J., Rushmeier, H., Áudio Silva, C., Taubin, G., & Member, S. (1999). *The Ball-Pivoting Algorithm for Surface Reconstruction*.
- Blomley, R., Weinmann, M., Leitloff, J., Jutzi, B., (2014). Shape distribution features for point cloud analysis – a geometric histogram approach on multiple scales *ISPRS Ann. Photogramm. Remote Sens. Spatial Inf. Sci.*, II-3, 9–1. <https://doi.org/10.5194/isprsannals-II-3-9-2014>
- Bolitho, M., Kazhdan, M., Burns, R., & Hoppe, H. (2009). *Parallel Poisson Surface Reconstruction*.
- Bolognesi, C. M., & Manfredi, V. (2024). Optimization of VR application in texturing Cultural Heritage. *The International Archives of the Photogrammetry, Remote Sensing and Spatial Information Sciences*, XLVIII- 2/W4-2024, 73–78. <https://doi.org/10.5194/isprs-archives-xxviii-2-w4-2024-73-2024>
- Buldo, M., Agustín-Hernández, L., Verdoscia, C., & R., T. (2023). A Scan-to-BIM workflow proposal for Cultural Heritage. Automatic point cloud segmentation and parametric-adaptive modelling of vaulted systems. *The International Archives of the Photogrammetry, Remote Sensing and Spatial Information Sciences – ISPRS Archives*, XLVIII (M-2), 333-340. <https://doi.org/10.5194/isprs-archives-XLVIII-M-2-2023-333-2023>
- Capone, M. & Lanzara, E. (2019): Scan-to-BIM vs 3D ideal model HBIM: parametric tools to study domes geometry, *The International Archives of the Photogrammetry, Remote Sensing and Spatial Information Sciences – ISPRS Archives*, XLII-2/W9, 219–226. <https://doi.org/10.5194/isprs-archives-XLII-2-W9-219-2019>
- Cicerchia, A., & Solima, L. (2021). The show must go on... line. Museums and their audiences during the lockdown in Italy. *SCIRES-IT - SCientific REsearch and Information Technology*, 11(1), 35–44. <https://doi.org/10.2423/i22394303v11n1p35>
- Clini, P., Mehtedi, M. El, Nespeca, R., Ruggeri, L., & Raffaelli, E. (2018). A digital reconstruction procedure from laser scanner survey to 3d printing: the theoretical model of the Arch of Trajan (Ancona). *SCIRES-IT - SCientific REsearch and Information Technology*, 7(2), 1–12. <https://doi.org/10.2423/i22394303v7n2p1>
- Cotella, V. A. (2023). From 3D point clouds to HBIM: Application of Artificial Intelligence in Cultural Heritage. *Automation in Construction*, 152(June), 10–11. <https://doi.org/10.1016/j.autcon.2023.104936>
- Crisan, A., Pepe, M., Costantino, D., & Herban, S. (2024). From 3D Point Cloud to an Intelligent Model Set for Cultural Heritage Conservation. *Heritage*, 1419–1437.
- Girardeau-Montau, D. (2020). *CloudCompare (version 2.12.alpha) [GPL software]*. Retrieved from <http://www.cloudcompare.org/>.
- De Fino, M., Porcari, V. D., Sciotti, A., Guida, A. and Fatiguso, F. (2022). Polychrome majolica of Apulian domes: history, technique, pathology, and conservation. *VITRUVIO - International Journal of Architectural Technology and Sustainability*, 7(2), 34–45. <https://doi.org/10.4995/vitruvio-ijats.2022.18684>

- Di Giuda, M. G., & Villa, V. (2016). *Il BIM - Guida completa al Building Information Modeling per committenti, architetti, ingegneri, gestori immobiliari e imprese*. Ulrico Hoepli Editore S.p.A.
- Digne, J. (2014). An Analysis and Implementation of a Parallel Ball Pivoting Algorithm. *Image Processing On Line*, 4, 149–168. <https://doi.org/10.5201/ipol.2014.81>
- Dimitrov, A., & Golparvar-Fard, M. (2015). Segmentation of building point cloud models including detailed architectural/structural features and MEP systems. *Automation in Construction*, 51(C), 32–45. <https://doi.org/10.1016/J.AUTCON.2014.12.015>
- Duda, R. O., & Hart, P. E. (1972). Use of the Hough Transformation to Detect Lines and Curves in Pictures. *Graphics and Image Processing*, 15(1), 11–15.
- Edelsbrunner, H., & Mucke, E. P. (1994). Three-Dimensional Alpha Shapes. *ACM Transactions on Graphics*, 13(1), 43–72.
- Fischler, M. A., & Bolles, R. C. (1981). Random Sample Paradigm for Model Consensus: An Application to Image Fitting with Analysis and Automated Cartography. *Graphics and Image Processing*, 24(6), 381–395.
- Florio, R., Catuogno, R., & Della Corte, T. (2019). The interaction of knowledge as though field experimentation of the integrated survey. The case of sacristy of Francesco Solimena in the church of san Paolo Maggiore in Naples. *SCIRES-IT - SCientific RESearch and Information Technology*, 9(2), 69–84. <https://doi.org/10.2423/i22394303v9n2p69>
- Grilli, E., Menna, F., & Remondino, F. (2017). A review of point clouds segmentation and classification algorithms. *International Archives of the Photogrammetry, Remote Sensing and Spatial Information Sciences - ISPRS Archives*, 42(2W3), 339–344. <https://doi.org/10.5194/isprs-archives-XLII-2-W3-339-2017>
- Grilli, E., & Remondino, F. (2019). Classification of 3D Digital Heritage. *Remote Sensing*, 11(7), 847. <https://doi.org/10.3390/rs11070847>
- Grilli, E., Farella, E. M., Torresani, A., & Remondino, F. (2019). Geometric features analysis for the classification of Cultural Heritage point clouds. *The International Archives of the Photogrammetry, Remote Sensing and Spatial Information Sciences - ISPRS Archives*, 42(2/W15), 541–548. <https://doi.org/10.5194/isprs-archives-XLII-2-W15-541-2019>
- Leserri, M., & Rossi, G. (2023). The digital documentation of the cultural heritage between public interest versus private property. Survey and research on the Immacolata Square in Martina Franca (Apulia, Italy). *SCIRES-IT - SCientific RESearch and Information Technology*, 13(2), 27–42. <https://doi.org/10.2423/i22394303v13n2p27>
- Kang, C. L., Wang, F., Zong, M. M., Cheng, Y., & Lu, T. N. (2020). Research on improved region growing point cloud algorithm. *The International Archives of the Photogrammetry, Remote Sensing and Spatial Information Sciences - ISPRS Archives*, 42(3/W10), 153–157. <https://doi.org/10.5194/isprs-archives-XLII-3-W10-153-2020>
- Kazhdan, M., Bolitho, M., & Hoppe, H. (2006). Poisson Surface Reconstruction. In *Eurographics Symposium on Geometry Processing*.
- Kazhdan, M., Klein, A., Dalal, K., & Hoppe, H. (2007). Unconstrained Isosurface Extraction on Arbitrary Octrees. In *Proceedings of the Fifth Eurographics Symposium on Geometry Processing* (pp.125–133). <http://dl.acm.org/citation.cfm?id=1281991.1282009>
- Khatamian, A., & Arabnia, H. R. (2016). Survey on 3D surface reconstruction. *Journal of Information Processing Systems*, 12(3), 338–357. <https://doi.org/10.3745/JIPS.01.0010>

Kyruakaki-Grammatikaki, S., Stathopoulou, E. K., Grilli, E., Remondino, F., & Georgopoulos, A. (2022). Geometric primitive extraction from semantically enriched point clouds. *The International Archives of the Photogrammetry, Remote Sensing and Spatial Information Sciences*. <https://doi.org/10.5194/isprs-archives-XLVI-2-W1-2022-291-2022>

Lanzara, E., Scandurra, S., Pulcrano, M., Acquaviva, S., Gallo, M., Palomba, D., & di Luggo, A. (2022). VPL for HBIM: Algorithmic Generative Processes for the Thematic Mapping of Information Models. *Springer Series in Design and Innovation*, 21(June), 453–463. [https://doi.org/10.1007/978-3-031-04632-2\\_47](https://doi.org/10.1007/978-3-031-04632-2_47)

Letard, M., Lague, D., Le Guennec, A., Lefevre, S., Feldmann, B., Leroy, P., Girardeau-Montaut, D., & Corpetti, T. (2024). 3DMASC: Accessible, explainable 3D point clouds classification. Application to bi-spectral topo-bathymetric lidar data. *ISPRS Journal of Photogrammetry and Remote Sensing*, 207, 175–197.

Liang, Y., Song, Q., Wang, R., Huo, Y., & Bao, H. (2023). Automatic Mesh and Shader Level of Detail. *IEEE Transactions on Visualization and Computer Graphics*, 29(10), 4284–4295. <https://doi.org/10.1109/TVCG.2022.3188775>

Musicco, A., Rossi, N., and Verdoscia, C. (2023). Accuracy evaluation of smartphone-based videogrammetry for Cultural Heritage documentation process. *The International Archives of the Photogrammetry, Remote Sensing and Spatial Information Sciences – ISPRS Archives XLVIII(M-2)*, 1119–1126, <https://doi.org/10.5194/isprs-archives-XLVIII-M-2-2023-1119-2023>

Pepe, M., Alfio, V. S., Costantino, D., & Scaringi, D. (2022). Data for 3D reconstruction and point cloud classification using machine learning in cultural heritage environment. *Data in Brief*, 42, 108250. <https://doi.org/10.1016/j.dib.2022.108250>

Pérez-Sinticala, C., Janvier, R., Brunetaud, X., Treuillet, S., Aguilar, R., & Castañeda, B. (2019). Evaluation of primitive extraction methods from point clouds of cultural heritage buildings. In *Structural Analysis of Historical Constructions* (Vol. 18, Issue February, pp. 1949–1958). [https://doi.org/10.1007/978-3-319-99441-3\\_250](https://doi.org/10.1007/978-3-319-99441-3_250)

Poux, F., Mattes, C., & Kobbelt, L. (2020). Unsupervised segmentation of indoor 3d point cloud: application to object-based classification. *International Archives of the Photogrammetry, Remote Sensing and Spatial Information Sciences - ISPRS Archives*, 44(4/W1), 111–118. <https://doi.org/10.5194/isprs-archives-XLIV-4-W1-2020-111-2020>

Rabbani, T., & Heuvel, F. Van Den. (2005). Efficient Hough transform for automatic detection of cylinders in point clouds. *ISPRS Proceedings Working Group V/I*, 60–65.

Saffi, H., Naima Otberdout, Hmamouche, Y., & Seghrouchni, A. E. F. (2024). Auto-BPA : An Enhanced Ball- Pivoting Algorithm with Adaptive Radius using Contextual Bandits. *IEEE/CVF Winter Conference on Applications of Computer Vision*, 3729–3737.

Sakamoto, M., Shinohara, T., Li, Y., & Satoh, T. (2020). Wall stone extraction based on stacked conditional gan and multiscale image segmentation. <https://doi.org/10.5194/isprs-archives-XLIII-B2-2020-1491-2020>

Schnabel, R., Wahl, R., & Klein, R. (2007). Efficient RANSAC for point-cloud shape detection. *Computer Graphics Forum*, 26(2), 214–226. <https://doi.org/10.1111/j.1467-8659.2007.01016>

Sharma, R., & Abrol, P. (2023). Parameter Extraction and Performance Analysis of 3D Surface Reconstruction Techniques. *International Journal of Advanced Computer Science and Applications*, 14(1), 331–336. <https://doi.org/10.14569/IJACSA.2023.0140135>

- Vosselman, G., & Dijkman, S. (2001). 3D building model reconstruction from point clouds and ground plans. *International Archives of Photogrammetry, Remote Sensing*, XXXIV(3), 38–43.
- Weinmann, M., Jutzi, B., Mallet, C., & Weinmann, M. (2017). Geometric features and their relevance for 3D point cloud classification. *ISPRS Annals of the Photogrammetry, Remote Sensing and Spatial Information Sciences*, 4(1W1), 157–164. <https://doi.org/10.5194/isprs-annals-IV-1-W1-157-2017>
- Yang, S., Shishuo X., and Wei H. (2022). 3D Point Cloud for Cultural Heritage: A Scientometric Survey. *Remote Sensing* 14(21), 5542. <https://doi.org/10.3390/rs14215542>
- Yang, S., Hou, M., & Li, S. (2023). Three-Dimensional Point Cloud Semantic Segmentation for Cultural Heritage: A Comprehensive Review. *Remote Sensing*, 15(3), 548. <https://doi.org/10.3390/rs15030548>
- Zhao, J., Hua, X., Yang, J., Yin, L., Liu, Z., Wang, X. (2023). A review of point cloud segmentation of architectural cultural. *The International Archives of the Photogrammetry, Remote Sensing and Spatial Information Sciences – ISPRS Archives (X-1/W1)*, 247–254. <https://doi.org/10.5194/isprs-annals-X-1-W1-2023-247-2023>